Non-Tracking Asymmetric Shadeless (NASH) Solar Collectors for Decarbonizing Industrial Process Heat

Yogesh Bhusal[1], Bennett Widyolar[1], Jordyn Brinkley[1], Mahmoud Abido[2], Roland Winston[1]
[1]Winston Cone Optics, Merced-CA (USA)
[2]University of California Merced-CA (USA)

Abstract

This work reports the development and year-long performance of an innovative non-tracking asymmetric shadeless (NASH) solar collector designed using nonimaging optics. The NASH collector can efficiently convert solar irradiance into thermal energy that is suitable for industrial process applications that need temperatures up to 200 °C. NASH design eliminates the need for row-to-row spacing as in conventional tilt-installed collectors and can be installed on ground and flat or slant roof without wasting any space. The collector has a nonimaging reflector that concentrates sunlight (from acceptance angle -75° to 5° from vertical) on the evacuated receiver tube with a geometric concentration ratio of 1.72X. Five early prototype modules are fabricated and tested for performance measurement. The collectors have demonstrated an optical efficiency of 58-60%, a peak efficiency of 50% while operating at 120 °C and full-year-average daily solar to thermal conversion efficiency of 42% for the year of 2022, while operating around 120 °C. The collectors were also tested at operating temperature of 150 °C and achieved solar-to-thermal conversion efficiency of >40%. The thermal energy generation of the collector at or near 120 °C ranged from 1 to 3.5 kWh/m^2/day over the year with lowest in winter months and highest in summer months.

Keywords: nonimaging optics, XCPC, NASH, solar thermal collector, solar thermal energy

1. Introduction

In 2021 out of 97.3 quadrillion BTUs (28516 TWh) total primary energy consumption in US, the industrial end use sector accounted for its 35% and was responsible for 30% of the total energy related CO_2 emissions in US. The majority (40%) of the energy consumption in the industrial sector is provided by natural gas and second to that (34%) by petroleum. Moreover, thermal energy consumption in industrial, residential and commercial sectors account for 23%, 7% and 4% respectively, of the total primary energy consumption in US (B. Widyolar et al. 2021). About 33% of this thermal energy consumed in industrial sector is utilized in process applications below 100 °C, about 44% between 100-500 °C, 13% between 500-1000 °C and 9% above 1000 °C (McMillan et al. 2021). Solar thermal energy technology is a promising renewable energy option to decarbonize these industrial thermal processes applications. In solar thermal energy technology, the more common flat plate collectors and evacuated tube collectors are mostly used for residential purposes and are not efficient at the temperatures above 80 °C and high-concentration solar thermal systems like PTC and Heliostat towers are economical only in large scale installations. Our team led by professor Roland Winston has developed and demonstrated the external compound parabolic concentrator (XCPC) technology since 2009 at the University of California Merced for applications like food processing (drying), wastewater evaporation and solar cooling with double effect LiBr absorption chiller.(B. Widyolar et al. 2021; Ferry et al. 2020; B. Widyolar et al. 2014; Milczarek et al. 2017; B. K. Widyolar et al. 2019). XCPC collectors are designed using nonimaging optics, can collect solar radiation throughout the day and year-round from a stationary position (non-tracking) and have no moving parts except for the pump for heat transfer fluid. During module level testing, at peak solar irradiance normally incident upon them, XCPCs have efficiently generated thermal energy at 100 °C and 200 °C at 60% and 50% solar to thermal conversion efficiency respectively(B. Widyolar et al. 2018).

In this work we report the development of an innovative variation of XCPC, called non-tracking asymmetric shadeless (NASH) collector which has an aperture parallel to the horizontal and can be installed flat on any surface without requiring row to row spacing. We have built and tested five prototype modules of the NASH collector each with an aperture area of 2.85 m^2 at UC Merced research facility in Atwater, CA. Among these five prototype modules, two modules are tested for a yearlong performance measurement while operating at ~120 °C, two modules are tested using vacuum intact (good vacuum) receiver tubes on one module and vacuum-lost (bad vacuum) receiver tubes on

Selection and/or peer review under responsibility of Scientific Committee
doi:10.18086/eurosun.2022.05.01 Available at http://proceedings.ises.org

the other module, for performance comparison while operating above 100 ºC and the fifth module is tested for stagnation with both good and bad vacuum receiver tubes. The NASH collector design including optical parametric optical simulations, FEA thermal fluid modeling and the experimental results of all three tests are discussed in this paper.

2. Collector Design

In this work we have redesigned the optics of external compound parabolic concentrator (XCPC) to develop an innovative stationary, non-tracking asymmetric shadeless (NASH) collector that is capable of efficiently converting solar irradiance into thermal energy up to 200 ºC. The original nonimaging XCPC collectors were installed in a conventional tilt design generally at latitude angle tilt, requiring the spacing between the rows to prevent the self-shading. The proposed new design NASH collector can be installed with horizontal aperture parallel to the ground/flat roof/slant roof (with some modification) and eliminates the need for spacing between the rows, thus allowing the land area that would otherwise be wasted to prevent row-to-row shading, to be utilized for active solar collection. This distinction between tilt collectors and proposed NASH collector is illustrated in **Figure 1 left**. No row-to-row spacing enables the equivalent-sized NASH solar collector array to be installed on a much smaller land footprint than the tilt design XCPC collectors. Moreover, this reduces the balance of system (BOS) costs by reducing the pipe lengths, insulation length, fluid volume thus reducing system warming up heat and heat losses from the longer pipes otherwise. The compact and low-profile flat installation causes low wind load on the collector and reduces structural design requirements against high winds. The NASH collectors can be installed on flat roof, slant roof, on ground and on façade without need for tilted frames. The collector modules are of robust construction made of Aluminum square tube framing and can be stacked on top of each other or be laid on their sides for transportation from one site to another. Also, the components can be easily disassembled and transported separately from one site to another site of installation.

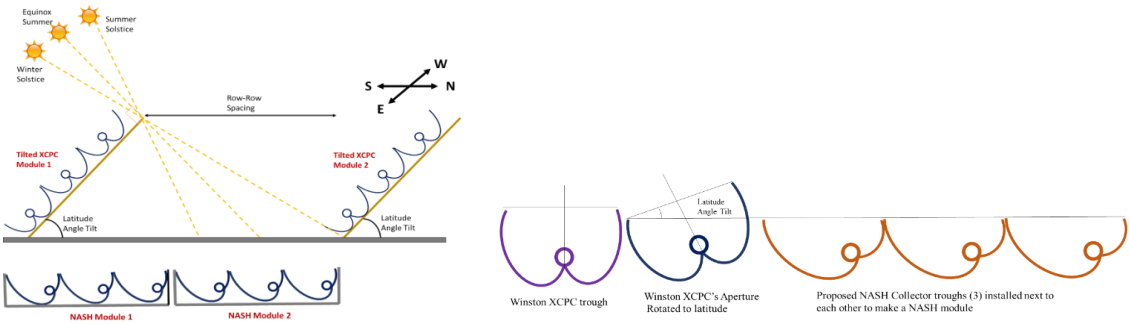

Figure 1.(left) Comparison of tilt installed XCPC collectors with row-to-row spacing and proposed shadeless NASH collector (right) Design steps of NASH collector.

The NASH design involves first generating the original XCPC trough for two inputs, a desired absorber diameter and acceptance angle, as described in the previous work (B. Widyolar et al. 2018; Winston, Jiang, and Ricketts 2018). Then the XCPC is rotated in an anticlockwise direction, usually at an angle equal to the latitude of the location to be installed on. Then the right-side reflector curve of XCPC is cut to the height of the left-side reflector curve to create horizontal aperture. Then the second similar trough can be placed next to the first one, in contact, without causing shading from the first trough, as illustrated in **Figure 1 right**. The shape of NASH collector shown in the paper does not represent the exact design curvature and is sketched only for illustration because of a patent in process.

A NASH collector module with a 2.85 m^2 aperture area has a gross land footprint of 3.64 m^2, giving the land fill-factor of 78%. Design specifications of a NASH module are listed in **Table 1**. **Figure 2** shows a CAD model and fabricated prototype of a three-tube NASH collector module. A NASH module has five major components- Frame, Reflector (3 troughs), Evacuated receivers (3 tubes) and Manifold. The reflector troughs and receivers are oriented in east-west directions just like the original XCPC collectors. Each trough's aperture can accept the sunlight between the acceptance angle of -75º to +5º due south from the vertical, enabling the collection of sunlight between the summer and winter solstice without any mechanical tracking. This angle is selected for NASH collector designed for latitude range (32-42º) of California USA but can be custom designed for any other latitude locations.

In each trough the nonimaging reflector of aperture 498 mm provides the geometric concentration of 1.72X at the 90 mm diameter absorber in metal-glass sealed vacuum receiver. The selectively coated Aluminum absorber fin (solar absorptance 95% and <8% infrared emittance) in the receiver tube absorbs 95% of the concentrated sunlight and limits the infrared re-radiation to less than 8% and the vacuum insulation in the receiver prevents the convection heat losses to the environment, thus ensuring efficient operation of the collector regardless of the ambient temperatures. The 80 inches long vacuum receiver is a borosilicate glass tube that houses a selectively coated low-cost Aluminum absorber fin in a decagon cross-section and a copper U-tube fluid channel that is ultrasonically welded to the inner surface of the absorber fin to ensure optimal conduction heat transfer from Aluminum absorber fin to the U-tube copper fluid channels. The reflectors are low-cost Aluminum sheet metal laminated by Mylar film and shaped to a nonimaging concentrator shape. These reflectors are paired with patented metal-glass vacuum receiver tubes and assembled on a robust Aluminum ribs and framing.

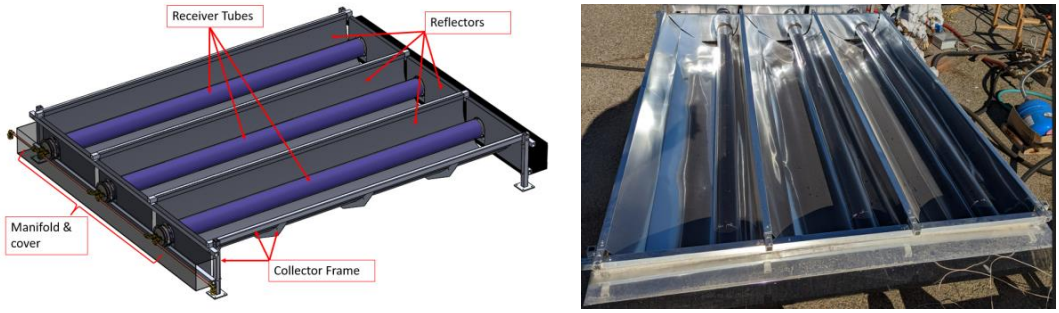

Figure 2. (left) Solid model of the NASH collector module and (right) prototype module.

Table 1. Design specifications of NASH collector module

Aperture area	2.85 m^2
Concentration ratio	1.72 X
Acceptance angle	±40° from 35° Latitude tilt or -75° to +5° from vertical
Troughs/tube length orientation	East-West
Land footprint/ Fill factor	3.64 m^2 / 78%
Collector height / weight	1 ft / 88 lbs
Working temperature	up to 200 °C

3. Performance Modeling

Firstly, a curvature of NASH reflector was generated using edge ray principle and string method of nonimaging optics by using the absorber size and acceptance angle and steps discussed in Design section. Then the corresponding optical model was created in a ray tracing simulation software, Light tools. **Figure 3** shows the optical model of the NASH collector trough of three design considerations: rotated and cut CPC (proposed design), full ACPC (alternative design) and half ACPC (alternative design). A parametric analysis was conducted to compute the shape efficiency or the intercept factor by considering ideal optical properties of reflector, glass tube and absorber, as a function of solar incidence angle from -90 to +90 degrees that represents the seasonal variation of the Sun's position in sky. An ideal solar collector will have shape efficiency/intercept factor of 1 for all angles within the acceptance angle. All three designs of NASH collector are developed to accept/collect the solar radiation incident from the range of -75° (rays coming from the left side of the vertical, representing solar incidence during equinox, winter solstice and most of the summer) to +5° (right side of the vertical, representing solar incidence during peak summer).

Again, the optical efficiency was also computed by assuming the incident light had a ±0.25° beam angle to approximate the solar disk angle, a reflector with 88% reflectance (Mylar film), a Borosilicate Glass tube envelope with Fresnel losses (4% loss on both glass surface) and the absorptance of the selectively coated absorber as 95%. The shape efficiency or intercept factor and optical efficiency of different designs of NASH collector are shown in plots in **Figure 4 and Figure 5.** The optical efficiency is the average of these shape efficiency/intercept factor at

different solar incidence angles within the acceptance angle range. The average optical efficiency of the NASH collector was computed to be 70%.

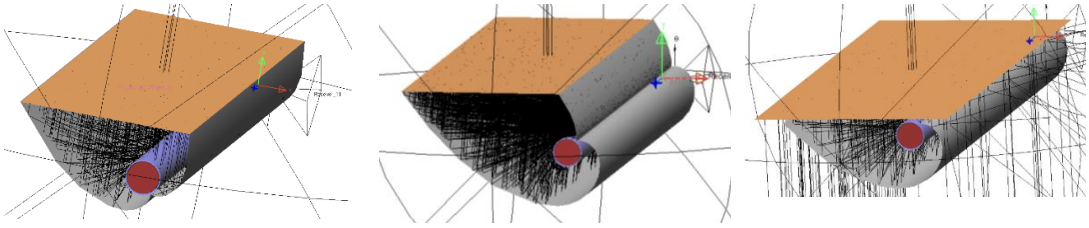

Figure 3. Ray-tracing simulations of different NASH collector designs: (left) Rotated and cut CPC, (middle) Full ACPC and (right) half ACPC

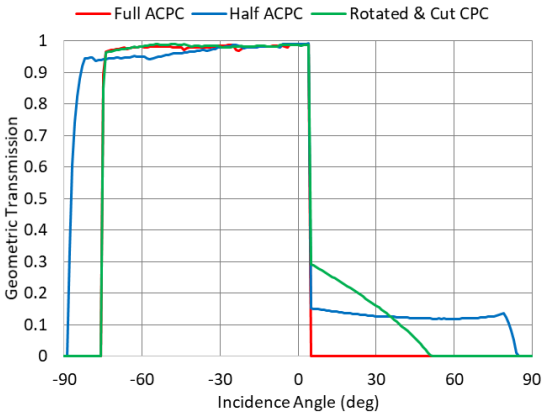

Figure 4. Intercept factor of different designs of NASH collector as a function of solar incidence angle

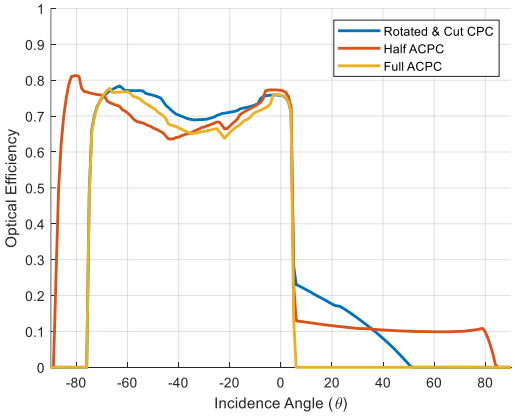

Figure 5. The optical efficiency of different designs of NASH collector as a function of solar incidence angles.

Using the average optical efficiency and the energy balance of incident solar power on to the absorber, thermal losses from the absorber at elevated temperature the theoretical thermal model of the NASH collector was developed and is shown in **Figure 6.** The plot shows the average optical efficiency from optical model (~70%) and the estimated solar to thermal energy conversion efficiency using the 25 g/s flow rate of 50/50 water/propylene glycol heat transfer fluid (HTF) under 1000 W/m^2 solar irradiance, at different working temperatures. The efficiency of the collector keeps decreasing as the working temperature increases and the collector stagnates (zero efficiency) at 370 ^{o}C. **Figure 7** shows the solar-to-thermal conversion efficiency plot of the proposed NASH collector at standard solar irradiance of 1000 W/m^2 and the lower levels of solar irradiances. The same collector will perform with lower thermal efficiency at the same temperature and will also stagnate at lower temperature. **Figure 8** shows the solar-to-thermal performance of NASH collector at solar irradiance of 1000 W/m^2 for varying flow rates of 50/50 water and propylene glycol. The curves show that the turbulence of HTF in the fluid channels is very important for efficient heat transfer from fluid channel walls to the HTF.

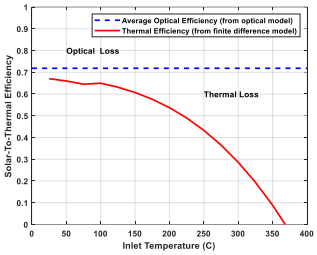

Figure 6. Modeled instantaneous solar-to-thermal efficiency of NASH collector with 25 g/s flow rate of 50/50 water/propylene glycol HTF under 1000 W/m^2 solar irradiance.

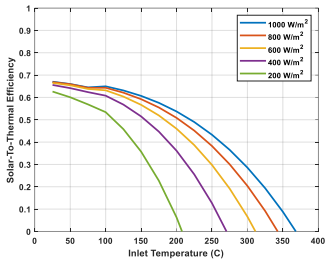

Figure 7. Solar-to-thermal performance of the NASH collector with a 25 g/s flow rate of 50/50 water/propylene glycol HTF under varying solar irradiance.

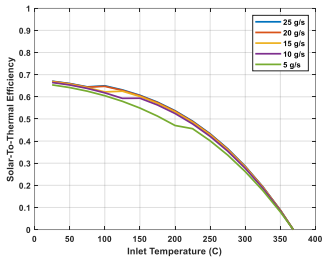

Figure 8. Solar-to-thermal performance of the NASH collector with 50/50 water/propylene glycol HTF under 1000 W/m^2 solar irradiance at varying flowrates.

Then, using the hourly solar resource data from TMY3 database for Merced, CA, an annual model was created which shows the daily solar energy available (solar insolation KWh/m^2/day), the solar energy absorbed by the collector at its optical efficiency also in (kWh/m^2/day) and the thermal energy generation (kWh/m^2/day) by the NASH collector while operating at 150 ^{o}C and are plotted in **Figure 9(left).** Moreover, the solar thermal power available, solar thermal power absorbed at optical efficiency and solar thermal power generated (at 150 ^{o}C) throughout the day in March 20, 21 and 22 of a typical year are shown in **Figure 9(right).** This thermal generation is obtained by subtracting the radiation losses from the collector at the operating temperature (here 150 ^{o}C) from the solar power absorbed by collector at its optical efficiency. The model does not consider the thermal losses from plumbing, storage tanks and other parasitic losses that depend on installations and thermal load types.

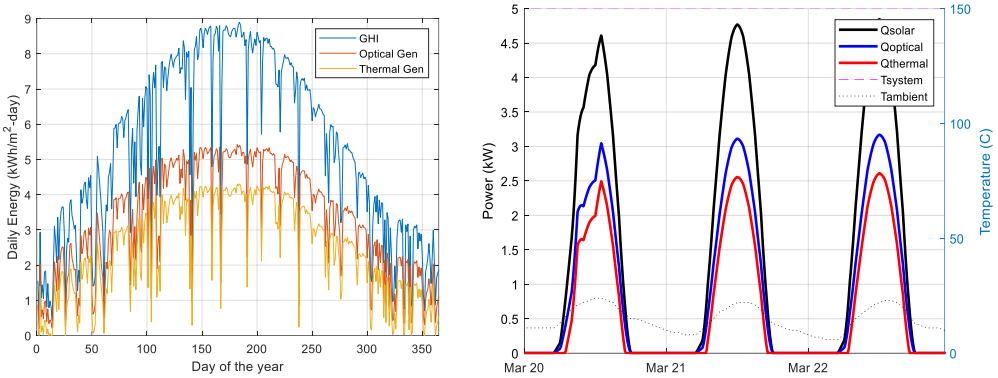

Figure 9. (left) Modeled daily available solar energy using TMY3 Global Horizontal Irradiance data, optical generation (energy absorbed by collector) and useful thermal energy carried by HTF while operating at 150 ^{o}C, all in KWh/m^2/day, from NASH collector in Merced, CA. (right) The solar incident power, absorber power and thermal generation (at 150 ^{o}C system operation) by two NASH modules (6 troughs, 6 tubes)

Moreover, FEA simulations were performed in COMSOL Multiphysics to determine the absorber fin material and the fin thickness. The thermal energy is generated at the absorber fin by the impingement of concentrated sunlight. This heat then transfers from the fin surface to the fluid channels (via conduction) through the 5 mm wide ultrasonic weld (contact surface of fluid channel and fin). Then the heat transfers from the inner surface of fluid channel to fluid by internal forced convection. The concentrated heat flux input was assigned to the specific boundary of the decagon absorber fin. The radiation boundary condition was applied to the full surface of the decagon absorber, the convection boundary condition (h) was applied to the inside surface of the fluid channels and the conduction was considered in all solids. The model was then meshed and computed for temperature distribution. The simulated stagnation temperature at the decagon shape absorber fin and U tubes are illustrated in **Figure 10** where it is seen that the highest temperature at absorber fin is 370 ^{o}C which is at the region of absorber fin where the sunlight is concentrated (at right surface of decagon fin) at vertical solar incidence and at the fluid channel is ~330 ^{o}C. **Figure 11** shows the temperature distribution at absorber fin and fluid channel when a 50 ^{o}C water flows through the fluid channel (copper tube) at 100 g/s. **Figure 12** shows the temperature distribution at absorber fin and fluid channel when a 200 ^{o}C duratherm oil is flowing through the collector at 100 g/s. There is approximately 40 ^{o}C temperature gradient

between the hottest spot in the absorber fin (a section of decagon absorber fin where concentrated sunlight impinges) and the U tube fluid channel. Eventually after conducting the FEA simulations and considering the much lower cost of Aluminum and yet its decent conductivity, an Aluminum absorber fin of 0.4 mm thickness and Copper U tube fluid channel of 6.5mm ID, 8 mm OD were selected for manufacture.

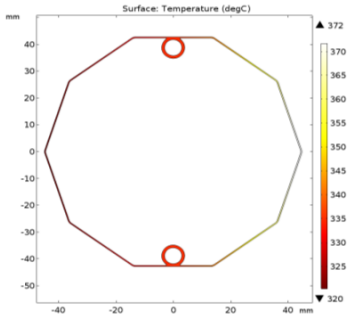

Figure 10. Stagnation temperature of aluminum fin and copper tube fluid channel

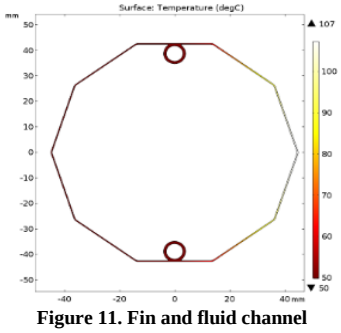

Figure 11. Fin and fluid channel temperatures as 50 ºC water flows through the tubes at 100 g/s

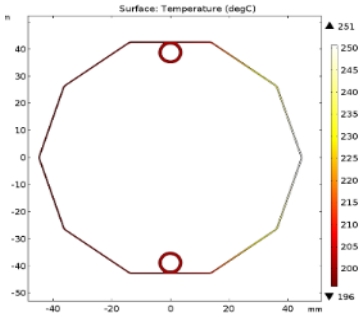

Figure 12. Fin and tube temperatures as 200 ºC duratherm oil flows through the tubes at 100 g/s

4. Experimental Results

4.1. Stagnation Temperature

To measure the highest collection temperature of the collector, a NASH module with one good vacuum receiver tube and two vacuum-lost receiver tubes, referred to as bad vacuum tube, was tested to stagnate on Sun with no heat transfer fluid moving through the collector, shown in **Figure 13**. In this case, the only heat lost by the absorber is the infrared thermal radiation emitted by the selective coated absorber in the vacuum tube. The top tube is non-evacuated and provides the maximum temperature achieved by a receiver tube that has lost its vacuum. The middle tube is evacuated, providing the maximum temperature achieved by the receiver tubes. Temperatures are measured using thermocouples directly inserted into the heat transfer fluid channels, so they are roughly in the middle of the tube, along the length. The evacuated tube has two thermocouples, one inserted in the receiver tube channel facing the short reflector length and one inserted into the opposite receiver tube channel facing the long reflector length (higher concentration ratio of light focused onto this side). The stagnation temperatures of these good and bad vacuum tubes were measured from June 8th to July 20th, 2022. The module under stagnation and the stagnation temperature data are shown in Figure 14. The evacuated receiver tube on a cleaned collector reached a maximum stagnation temperature of up to 330 ºC and remained >300 °C even on partly cloudy days and with dusty reflectors. The bad vacuum or non-evacuated tube reached a temperature of about 230 °C.

We performed a more than a month-long stagnation test of the collector as destructive testing to understand the worst-case operating condition of the collector. In real world installation, the solar thermal array and the heat transfer fluid loop should be engineered to avoid stagnation. Stagnation of solar thermal array can occur if the HTF pump stops either due to power outage or pump failure. This causes the stagnant overheating of heat transfer fluid and extreme pressures build up inside the collectors' fluid channels and fluid handling system. This could cause undesirable thermal loop expansion, a plumbing system failure, equipment failure and personal injury. The stagnation control strategy such as installation of mechanical pressure relief valve (PRV) at the outlet is important to prevent system failure due to pump-failure stagnation. Whereas sometimes the high temperatures can build up when heat transfer fluid cannot dump heat to the load. In this case, a temperature control heat dump (radiator and fan) should be installed to control the temperature rise in the solar array.

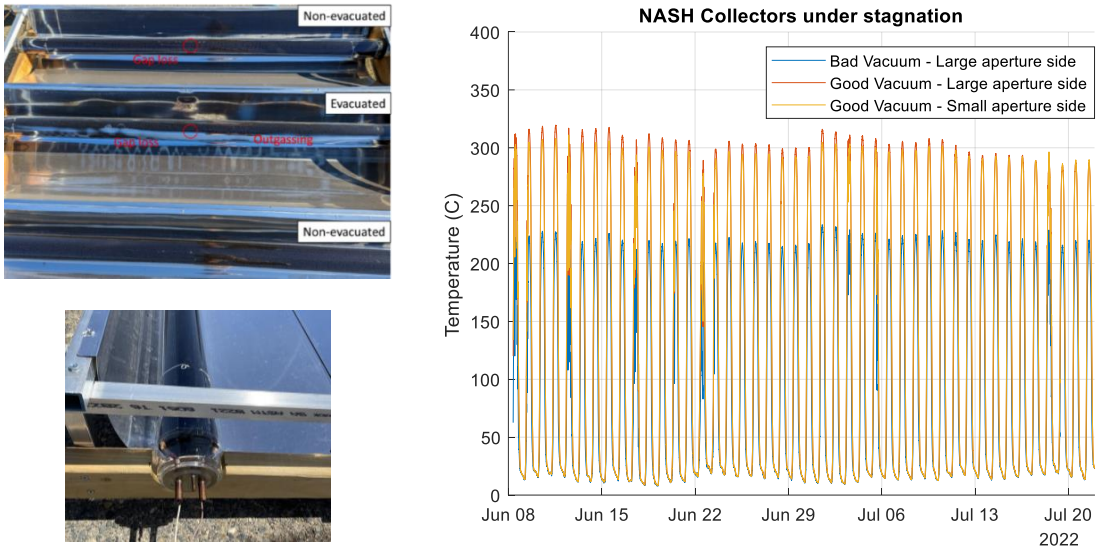

Figure 13. (left) A NASH module with two bad vacuum receiver tubes and one good vacuum receiver tube under stagnation test, and closeup of thermocouple wires inserted into a receiver tube and (right) the stagnation temperature plot.

4.2. First Two Prototype Modules (Full Year Testing)

The first two prototype modules (Aperture area 2 x 2.85m^2=5.7 m^2) of NASH collectors were connected in series and set for long-term performance measurement while operating above 100 ^{o}C. **Figure 14** shows the first and second prototypes of NASH collectors undergoing long-term testing. A solar circulating pump station (SRS-145-5.1) is used to circulate the heat transfer fluid(water) through the collectors and internal copper heat exchanger coils in the 53-gallon solar hot water tank (DUDA Solar). The pump control system turns the pump on every morning when the solar sensor measures the irradiance of 150 W/m^2 or if the solar loop fluid goes below 0 ^{o}C (for freeze protection) and keeps the pump turned off otherwise. During sunny hours, the water in the tank is indirectly heated by the HTF in heat exchanger coils. The water in the tank is free to evaporate out of the tank-top opening to the atmosphere as it is heated to 100 ^{o}C by the circulating HTF. The mass flow rate in the loop is measured by using a Coriolis flowmeter with frequency output. A PSP solar sensor (voltage output) placed on the same horizontal plane as the collector aperture measures the incoming Global Horizontal Irradiance (GHI). Temperatures at the collector inlet/outlet and tank inlet/outlet are measured by thermocouples directly inserted into the flow path. The data is logged every 5 seconds using the DI 808 web-based data logger from DATAQ instruments. Loop pressure was measured using an absolute pressure transmitter with a 0-5 V signal output.

Figure 14. Prototype 1 and 2 undergoing long-term testing at temperatures >100 ^{o}C

Every 5 seconds, the GHI, collector inlet/outlet temperatures and flowrate are recorded. The thermal power absorbed by the HTF is calculated by the product of mass flow rate, specific heat capacity and temperature rise in the collector inlet/outlet. The thermal power absorbed is divided by the incident solar power (product of GHI and collector aperture) to give the instantaneous solar to thermal conversion efficiency.

$$\eta = \frac{mc_p(T_o - T_{in})}{\text{GHI} * \text{Collector Aperture Area}} \qquad \text{(eq. 1)}$$

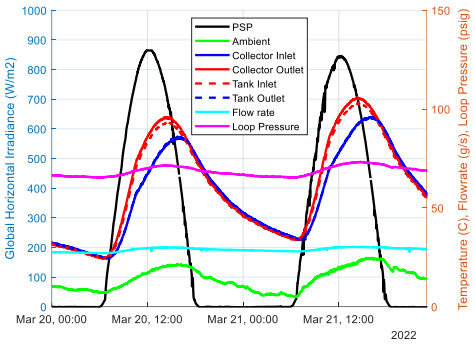

Figure 15. Instantaneous plot of GHI, collector and tank inlet/outlet temperatures, mass flowrate and loop pressure

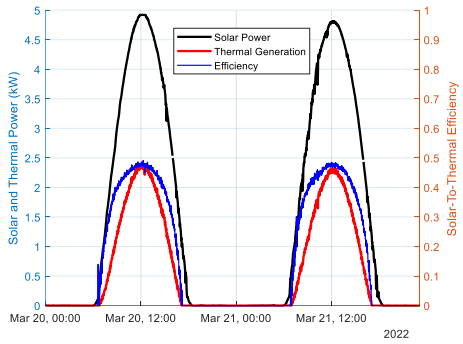

Figure 16. Instantaneous plot of incident solar power, thermal power generated and the instantaneous efficiency.

Figure 15 and **Figure 16** show the instantaneous plots of operating temperatures and instantaneous incident solar power, thermal power generated by the collector and the instantaneous efficiency of the collector. Then for each full day, the area under the thermal generation curve (power x timestep = kWh) is divided by the area under incident solar power (also in kWh) to obtain the solar to thermal conversion efficiency of that day, called daily efficiency. For each month these daily efficiencies and other measurements were consolidated and plotted for the full month starting in Figure 18. The left plot on each figure shows the daily data such as maximum ambient temperature, maximum temperature on solar HTF, maximum tank temperature, maximum and minimum loop pressure, and maximum wind speed. The right plot shows the solar insolation (KWh/m^2) measured every day.

Figure 17 shows the performance data measured during the month of January. Due to the ambient temperature below 0 ºC during January, the loop did not go above 100 ºC except during one temporary stagnation that recorded higher temperature. Average daily efficiency for the month of January was 49%.

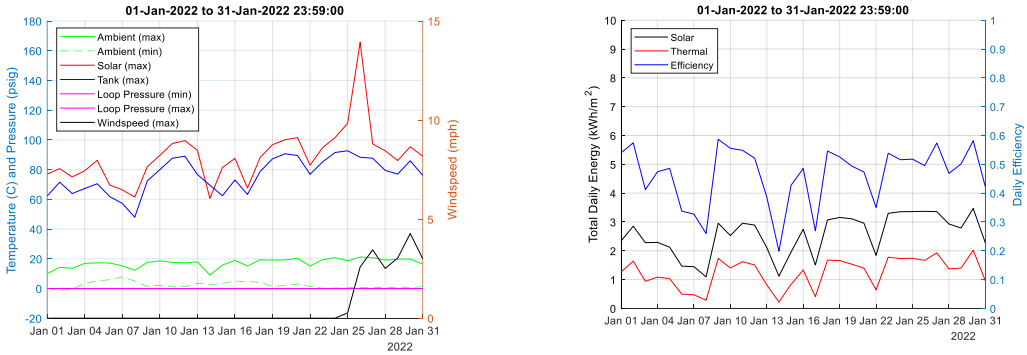

Figure 17. January performance measurement

Figure 18 shows the performance in June, which was also as expected, and the average daily efficiency in June was 42%.

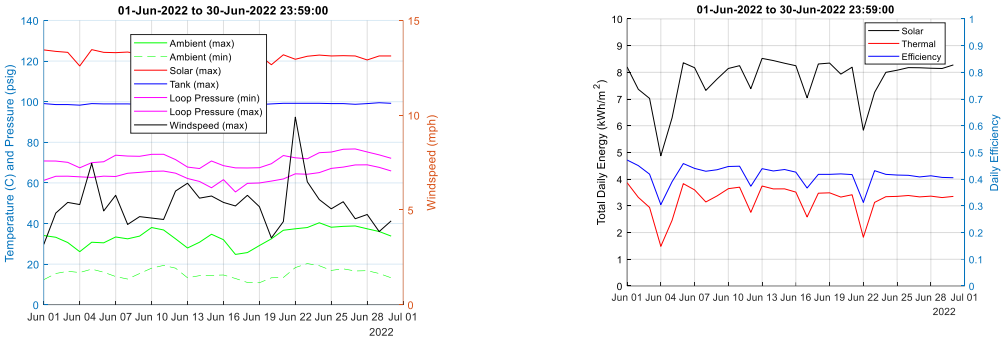

Figure 18. June performance measurement

Figure 19. shows the performance in July, which was also as expected, and the average daily efficiency in July was 45%.

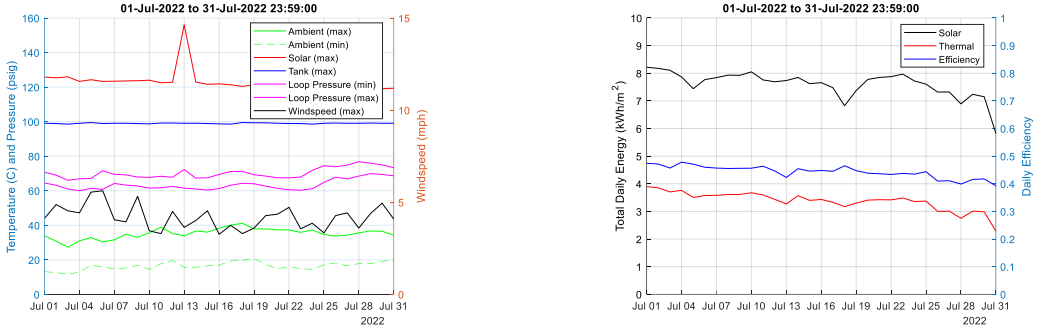

Figure 19. July performance measurement

These measurements were recorded for each day in the year 2022 starting January 01 to Dec 31. The collectors were cleaned on the first day of each month. The monthly averages of modelled solar, measured solar, modelled thermal generation, measured thermal generation are also calculated and plotted in **Figure 20**. It seems that thermal energy generation by NASH collectors (purple line) ranges between **1 kWh/m^2/day** in the winter months to upto **3.5 kWh/m^2/day** in summer months. The measured thermal generation seems to be approximately equal to 42% of total measured solar insolation (GHI), which is shown as new model curve. Due to the horizontal aperture NASH collector collects maximum solar insolation during the summer months when the cosine effects are minimum. The daily thermal energy generation by the NASH collector averaged over 365 days was 2.16 kWh/m^2/day, which means 1 square meter aperture of NASH collector will generate **~800 kWh** of thermal energy at or near 120 ºC, over a full year. The daily solar insolation in test location in Atwater, California averaged over all 365 days was 5.16 kWh/m^2/day.

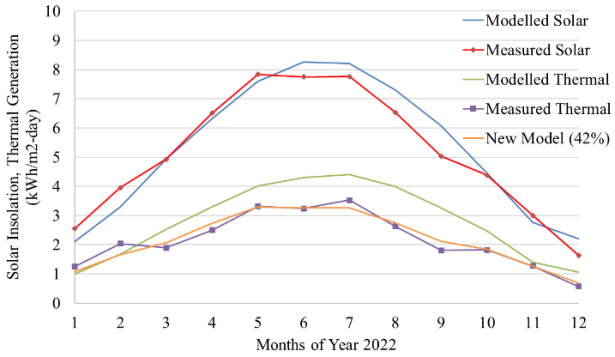

Figure 20. A yearlong performance of 2 modules of NASH collectors

The NASH collector module performance turned out to be 77% of the originally modelled performance. The 23% difference can be attributed to the optical transmission losses due to fabrication and assembly errors, soiling in reflectors and glass tube, heat losses from manifold and lower than modelled solar irradiance. In January and February, it is seen that the collector is producing more than expected because in these winter months, the collector was operating under 100 ºC and was producing more energy than modeled for operating at 120 ºC.

4.3. Third & Fourth Prototype- Good Vacuum and Bad Vacuum Test

A separate test loop was set up for performance measurement of the third and fourth prototype modules. The experiment aimed to understand the difference in the performance of module #1 good vacuum collector and module #2 bad vacuum collector at temperatures as high as 150 ºC. The test loop setup is shown in **Figure 21,** and the test started in June 2022. Module #1 on the right has three evacuated receiver tubes and module #2 in the left has three non-evacuated receiver tubes. A preheater calorimeter is installed before the collector modules such that the calorimeter, module #1 and module #2 are plumbed in series. The heat transfer fluid (Water) first goes through Calorimeter, then to the good vacuum tube collector, then to the bad vacuum tube collector, and recirculates, thus has a same flow rate for all three systems. The thermocouples were placed at inlet/outlet of calorimeter, outlet of module #1 and outlet of module #2. The thermocouple at outlet of the calorimeter would serve as the inlet temperature of the fluid entering the good-vacuum module. The outlet of the good-vacuum module would be an inlet of the bad-vacuum module. Finally, the outlet temperature of the bad vacuum modules was measured. Also, the Global Horizontal Irradiance was measured by the PSP placed at the horizontal plane. The calorimeter served as the flow rate measurement device. By measuring the current (I_c) and voltage (V_c) at the calorimeter terminals, using their product as input thermal power, and using specific heat capacity of water and using the inlet and outlet temperatures at calorimeter, we could calculate the flow rate in the loop. The calorimeter was insulated and assumed that the electrical power in the calorimeter was fully converted to heat.

To account for any heat loss from the calorimeter or the thermal energy not transferred to the fluid going through calorimeter, we measured the temperature gained by fluid across the calorimeter inlet/outlet while Calorimeter is on and measured the temperature drop of fluid across the calorimeter inlet/outlet while Calorimeter is intentionally turned off and added these and equated with the Calorimeter input electrical power. This will give us the accurate mass flowrate across the loop. The temperature drop across the calorimeter while it is turned off during high-temperature operation is essentially the heat loss from the calorimeter at that temperature, which is not actually being utilized even while it is turned on and hence should be deducted from the calorimeter power (IV) to accurately calculate flow rate.

$$I_c V_c = \left(mc_p(Tc_o - Tc_i)\right)_{\text{Cal on}} + \left(mc_p(Tc_i - Tc_o)\right)_{\text{cal off}} \qquad \text{(eq. 2)}$$

By calculating the flow rate from the above equation, the instantaneous solar thermal efficiency of both good vacuum and bad vacuum collectors were calculated using the temperature rise across these modules.

$$\eta = mc_p(T_o - T_{in})\ /\text{GHI} * \text{Collector Aperture Area} \qquad \text{(eq. 3)}$$

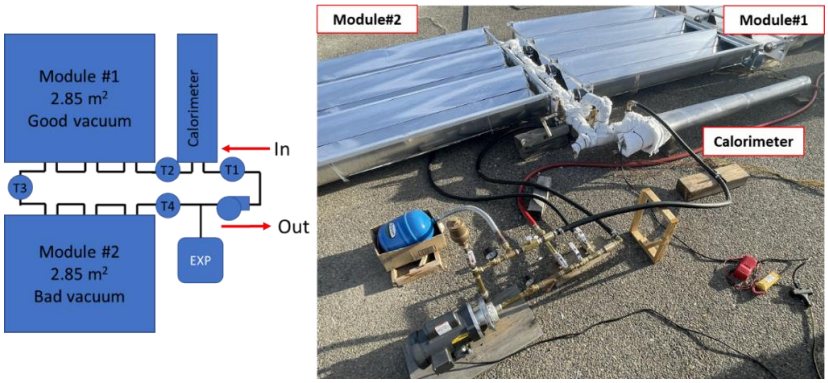

Figure 21. East-west oriented third and fourth prototype NASH collector modules during on-Sun test with Calorimeter.

The efficiency is plotted against mean temperature of the collector (the average of the collector inlet and outlet) and against the reduced temperature (T*) as shown in **Figure 22 (left) and (right)** respectively. Reduced temperature $T^* = \frac{T_m - Ta}{GHI}$ where T_m is a collector mean temperature (average of inlet and outlet temperatures) is a normalized temperature parameter that incorporates the combined effects of operating temperature, ambient temperature, and variable solar radiation to the instantaneous efficiency. The instantaneous efficiency of solar thermal collectors is generally plotted against this parameter. The collector demonstrated an efficiency >40% at temperatures above 100 ºC and up to 150 ºC. We can also see that the vacuum integrity of the receiver tubes is very important for efficient operation of the collectors. The distinction in the performance of good and bad vacuum collectors can be seen even at the operating mean temperature of 50 ºC. The efficiency of a bad vacuum module is significantly lower than that of a good vacuum module beyond operating temperatures of 100 ºC.

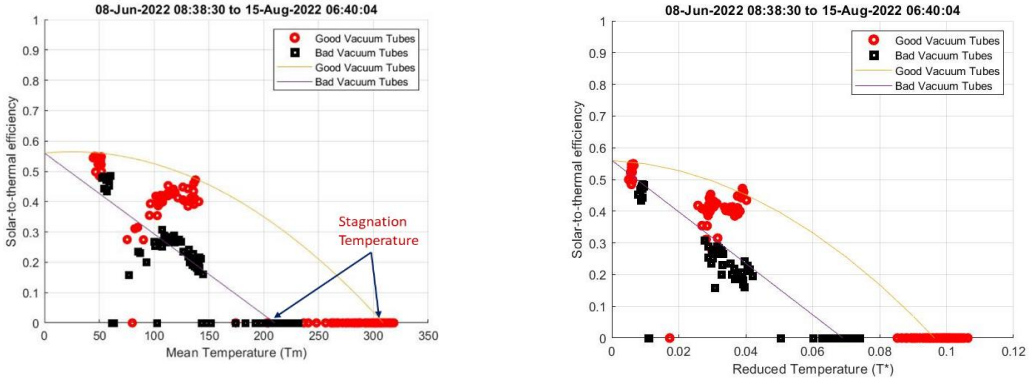

Figure 22. (left) Thermal efficiency at different mean fluid temperature, for good vacuum and bad vacuum collectors and (right) thermal efficiency as a function of reduced temperature parameter.

To summarize, in all five prototype modules we notice that the measured efficiency is lower than the modeled efficiency. This is mainly because of the imperfections in the reflector fabrication, meaning the exactness of reflector curvature. Imperfect reflector curvature reflects the incoming solar radiation away from the absorber thereby reducing the optical efficiency. The modeled optical efficiency was about 70%. However, the measured optical efficiency is around 56-58%. As the operating temperatures go higher, the solar-to-thermal energy conversion efficiency reduces due to thermal radiation loss from the collector. In **Figure 23** we can see the blue color of the sky on the reflectors instead of the dark blue color of the absorber. This means that the light incident on those sky-blue parts of the collector from your viewing angle or camera angle will not be directed to the absorber and will be reflected to the sky. Furthermore, soiling is a very important factor that reduces the efficiency of the collector, especially when the collectors are installed around dusty environments like farmland and construction regions. In addition to the working temperature, the efficiency can be impacted by ambient temperature, wind conditions, incident solar irradiance and dust level on the collector; hence, the efficiency is not consistent even for the same operating temperatures on different days.

Figure 23. Gap losses and other optical losses due to reflector imperfections in NASH prototype modules.

5. Conclusion

We presented optical design and modeling and thermal performance modeling of the NASH collector at elevated temperatures. The NASH collector could readily achieve the optical efficiency of ~65-70% if they are developed using standard manufacturing methods where the optical imperfections due to fabrication errors and gap losses are avoided. Moreover, we presented the results of experimental testing of prototypes 1 & 2, 3 & 4, and 5. We reported that the NASH collector with 1.72X concentration ratio achieved a stagnation temperature of up to 330 ^{o}C, optical efficiency of 56-58% (on early prototypes), an instantaneous peak efficiency of 50% while operating at 120 ^{o}C and average daily efficiency of 42% in the Year 2022, while operating around 120 ^{o}C. In the good vacuum versus bad vacuum module testing the NASH collectors operated between 100 ^{o}C and 150 ^{o}C and achieved solar-to-thermal conversion efficiency of >40%. We understood from the good vacuum and bad vacuum modules experiment that the vacuum integrity is crucial at high temperatures for efficient operation, however, bad vacuum tubes collector still can provide positive heat generation at temperatures up to 230 ^{o}C. These prototype modules had optical imperfectness due to early-stage fabrication methods that can be improved in the future. We have not observed any problems with the collectors in the instances of weather conditions like snowing in Winter, high winds on test site recorded up to 55 mph and stagnation with HTF measuring up to 260 ^{o}C and high pressure (100 psi relief valve). The team is working towards employing low-cost materials and manufacturing methods to reduce the Levelized cost of heat (LCOH) of these collector systems.

6. Acknowledgment

This work has been funded by California Energy Commission (CEC), USA under the grant number PIR-20-004. The authors are thankful to Robyn Lukens for her contribution to this research project.

7. References

Ferry, Jonathan, Bennett Widyolar, Lun Jiang, and Roland Winston. 2020. “Solar Thermal Wastewater Evaporation for Brine Management and Low Pressure Steam Using the XCPC.” *Applied Energy* 265 (December 2019): 114746. https://doi.org/10.1016/j.apenergy.2020.114746.

McMillan, Colin, Carrie Schoeneberger, Jingyi Zhang, Parthiv Kurup, Eric Masanet, Robert Margolis, Steven Meyers, Mike Bannister, Evan Rosenlieb, and William Xi. 2021. “Opportunities for Solar Industrial Process Heat in the United States. (Under Review).,” no. January: NREL/TP-6A20-77760.

Milczarek, Rebecca R., Jonathan J. Ferry, Fatima S. Alleyne, Carl W. Olsen, Donald A. Olson, and Roland Winston. 2017. “Solar Thermal Drum Drying Performance of Prune and Tomato Pomaces.” *Food and Bioproducts Processing* 106 (November): 53–64. https://doi.org/10.1016/J.FBP.2017.08.009.

Widyolar, B.K., L. Jiang, J. Ferry, J. Brinkley, Y. Bhusal, and R. Winston. 2019. “Nonimaging Solar Collectors toward Net-Zero GHG Emission.” In *Proceedings of SPIE - The International Society for Optical Engineering*. Vol. 11120. https://doi.org/10.1117/12.2534513.

Widyolar, Bennett, Lun Jiang, Yogesh Bhusal, Jordyn Brinkley, and Roland Winston. 2021. “Solar Thermal Process Heating with the External Compound Parabolic Concentrator (XCPC) – 45 m 2 Experimental Array Performance , Annual Generation (KWh / m 2 -Year), and Economics.” *Solar Energy* 230 (July): 131–50. https://doi.org/10.1016/j.solener.2021.10.027.

Widyolar, Bennett, Lun Jiang, Jonathan Ferry, and Roland Winston. 2018. “Non-Tracking East-West XCPC Solar Thermal Collector for 200 Celsius Applications.” *Applied Energy* 216 (January): 521–33. https://doi.org/10.1016/j.apenergy.2018.02.031.

Widyolar, Bennett, Roland Winston, Lun Jiang, and Heather Poiry. 2014. “Performance of the Merced Demonstration XCPC Collector and Double Effect Chiller.” *Journal of Solar Energy Engineering, Transactions of the ASME* 136 (4): 1–13. https://doi.org/10.1115/1.4027726.

Winston, Roland, Lun Jiang, and Melissa Ricketts. 2018. “Nonimaging Optics: A Tutorial.” *Advances in Optics and Photonics* 10 (2): 484. https://doi.org/10.1364/AOP.10.000484.